New approach to polarization phenomena in dp backward elastic scattering at intermediate and high energies

M. Tanifuji and S. Ishikawa
Department of Physics, Hosei University, Fujimi 2-17-1, Chiyoda, Tokyo 102, Japan

Y. Iseri
Department of Physics, Chiba-Keizai College, Todoroki-cho 4-3-30, Inage-ku, Chiba 263, Japan
(Received 29 December 1997)

The spin observables T_{20}, $\kappa_0=\frac{3}{2}K_y^y$ $(d\rightarrow p)$, K_{xz}^y, K_y^y $(p\rightarrow p)$, and C_{yy} are investigated for dp backward elastic scattering at intermediate and high energies by the invariant-amplitude method with the one-nucleon-exchange assumption. Recently observed discrepancies between the conventional calculations and the experimental data for the κ_0-T_{20} correlation are mostly dissolved by including effects of imaginary parts as the contribution of absorption in the invariant amplitudes. The dependence of the measured T_{20} and κ_0 on the proton-neutron relative momentum is explained by the calculation with the specification of nuclear potentials, except T_{20} at high energies, for which possible solutions are investigated. Clear dependence on the imaginary parts of the amplitudes is found for K_{xz}^y, measurements of which are suggested to be useful to distinguish between the solutions. [S0556-2813(98)06605-9]

PACS number(s): 21.30.−x, 21.45.+v, 24.70.+s, 25.10.+s

I. INTRODUCTION

Polarization phenomena in few-body systems are important sources of information on nuclear forces and related dynamics. In backward elastic scattering of deuterons by protons, the structures of the cross section σ and the tensor analyzing power T_{20} experimentally observed at $E_d=0.5-1$ GeV [1] attracted attention as the signal of excitations of the related nucleons to baryon resonance states, for example to the Δ states [1–4], although the problem has not yet been solved, in particular, from a quantitative point of view. Recently, discrepancies between T_{20} and κ_0 $(=\frac{3}{2}K_y^y$, $d\rightarrow p$ vector polarization transfer coefficient) measured by experiments and those calculated by the PWIA have been emphasized in the form of the correlation between these quantities. That is, the quantities calculated by the PWIA with the one nucleon exchange (ONE) model [5], which describes the dominant mechanism at the backward angle in the high energy region, satisfy the equation of a circle in the κ_0-T_{20} plane [6], while the measured ones deviate remarkably from the circle along a spiral-like curve [7]. The observables for the inclusive deuteron breakup also suffer from similar difficulties [7]. These suggest the possibility of finding new aspects of the nuclear force by detailed investigations of the scattering, since the system consists of only three nucleons and ambiguities due to many bodies are less important. Sophisticated calculations [8–10], which include relativistic effects or QCD ones for example, have not been successful in explaining the experimental data and the puzzle still remains to be unsolved.

As a new approach to the problem, we will derive general formulas of the spin observables T_{20}, κ_0, K_{xz}^y $(d\rightarrow p$ tensor-to-vector polarization transfer coefficient), K_y^y $(p\rightarrow p$ vector polarization transfer coefficient), and C_{yy} (spin correlation coefficient), for the dp backward elastic scattering by the invariant-amplitude method [11] with the ONE assumption. In the method, we expand the scattering T matrix by tensors in the spin space to calculate the geometrical parts of the matrix elements in a simple way. Then physical quantities are represented by the physical parts of the matrix elements, which we call the invariant amplitude due to the invariance character for rotations of the coordinate axes. The spin observables are described with relative magnitudes and phases between the amplitudes. The formulas of the observables thus obtained are independent of details of the reaction dynamics except for the limitation due to the ONE assumption. In general, effects of reaction channels other than the elastic scattering will mainly be included in the imaginary part of the scattering amplitude as absorption effects. Then we investigate general effects of the imaginary part of the invariant amplitudes on the spin observables by treating the relative phases, which are fixed to zero or π in the PWIA, as free parameters. In the numerical calculation, the magnitudes of the amplitudes are tentatively evaluated by the PWIA with the ONE assumption and corrections are included. Therefore, the present calculation is more general than the PWIA. Recently, formulas of T_{20} and κ_0, which are model-independent, have been derived for special (d,p) reactions where one of the target and residual nuclei is spinless and the other is spin-1/2 [12]. The present theory is an extension of that work.

The main results in the present paper are as follows. The imaginary parts of the amplitudes produce important effects on the observables and most of the discrepancies in the κ_0-T_{20} correlation can be dissolved by the effects. The dependence of the measured T_{20} and κ_0 on the proton-neutron relative momentum k is very well reproduced by the present calculation except T_{20} at high momenta, which correspond to high incident energies [4], $k\geqslant 0.7$ GeV/c. To reproduce the high-energy data, several solutions are discussed as candidates where momentum-dependent corrections to the magnitude of the amplitude, the participation of exotic phenomena

and an improvement of nuclear potentials are considered. It is shown that K_{xz}^{y} is particularly sensitive to the imaginary amplitude and is useful in distinguishing between the solutions when the quantity is measured.

In Sec. II, the general formulas of the spin observables are derived by the invariant-amplitude method with the assumption of the ONE mechanism. In Sec. III, the κ_0-T_{20} correlation data are analyzed by the formulas without introducing particular nuclear potentials. In Sec. IV, the k dependence of the spin observables is investigated using the deuteron internal wave functions obtained by specifying the nuclear potential. Finally, Sec. V is devoted to a summary and discussions.

II. DERIVATION OF FORMULAS OF SPIN OBSERVABLES

The T-matrix $\boldsymbol{M}$ can be expanded into tensors in the spin space, say $\boldsymbol{S}_{K\kappa}$,

$$\boldsymbol{M}=\sum_{K\kappa}(-1)^{\kappa}\boldsymbol{S}_{K-\kappa}\boldsymbol{R}_{K\kappa}, \tag{1}$$

where $\boldsymbol{R}_{K\kappa}$ is the counter part, the tensor in the coordinate space, and $K(\kappa)$ designates the rank (z component) of the tensor. This form has an advantage in classifying the T-matrix elements according to their tensorial properties in the spin space. Explicitly, the scalar part ($K=0$) describes scattering amplitudes due to central interactions, the vector one ($K=1$) those due to spin-orbit interactions and the tensor one ($K=2$) those due to tensor interactions. The last one includes effects of D-components of the internal states of the related particles. The interaction associated with each rank includes higher-order effects of interactions as long as the tensorial property is maintained.

The matrix element of Eq. (1) is given for a reaction $aA\rightarrow bB$ by the invariant-amplitude method [11]. There, the matrix element was derived in the nonrelativistic framework but it can be applied to the relativistic energy region when spins of the related particles are treated in the helicity frame. In the present case, the transformation of the frame for the high-energy application does not produce any essential change in the result, since we are concerned with the backward scattering. Following Ref. [11],

$$\begin{aligned}\langle \nu_b,\nu_B;\boldsymbol{k}_f|\boldsymbol{M}|\nu_a,\nu_A;\boldsymbol{k}_i\rangle=&\sum_{s_i s_f K}(s_a s_A \nu_a \nu_A|s_i\nu_i)\\&\times(s_b s_B \nu_b \nu_B|s_f\nu_f)\\&\times(-1)^{s_f-\nu_f}(s_i s_f \nu_i-\nu_f|K\kappa)\\&\times\sum_{l_i=\bar{K}-K}^{K}[C_{l_i}(\hat{k}_i)\\&\otimes C_{l_f=\bar{K}-l_i}(\hat{k}_f)]_{\kappa}^{K}F(s_i,s_f,K,l_i),\end{aligned} \tag{2}$$

where $\boldsymbol{k}_i$ ($\boldsymbol{k}_f$) is the relative momentum in the initial (final) state and $s(\nu)$ denotes the spin (z component). The quantity $\hat{k}_i$ ($\hat{k}_f$) is the solid angle of $\boldsymbol{k}_i$ ($\boldsymbol{k}_f$) and C_{lm} is related to Y_{lm} as usual. The matrix element of $\boldsymbol{S}_{K-\kappa}$ is calculated by the Wigner-Eckart theorem and the geometrical part is given by the Clebsch-Gordan coefficients in Eq. (2). The geometrical part of the matrix element of $\boldsymbol{R}_{K\kappa}$ will be represented by $[C_{l_i}(\hat{k}_i)\otimes C_{l_f}(\hat{k}_f)]_{\kappa}^{K}$ since the matrix element is a tensor constructed of ordinary-space vectors and we have only two such vectors, $\boldsymbol{k}_i$ and $\boldsymbol{k}_f$, after the integration over the coordinate variables. The physical parts of both matrix elements are included in $F(s_i,s_f,K,l_i)$. This quantity is invariant under rotations of the coordinate axes and we will call $F(s_i,s_f,K,l_i)$ the invariant amplitude, which is a function of scattering angle θ and the center-of-mass energy. The quantity $\bar{K}$ is K for $K=$ even and $K+1$ for $K=$ odd in the present case. More details are given in the appendix of Ref. [11].

For the backward scattering, we have four independent matrix elements [10], among which $\langle 1,-\frac{1}{2}|\boldsymbol{M}|1,-\frac{1}{2}\rangle$ is assumed to vanish for the ONE mechanism, where the initial proton forms the final deuteron with the neutron of the incident deuteron. In the present case, the spin-down proton in the incident channel cannot form the spin-up deuteron in the final channel without spin flips of the proton and the spin flip does not occur at the backward angle in the PWIA limit [6]. This assumption decreases the number of the independent amplitudes and finally we get other three matrix elements by Eq. (2) as

$$\left\langle 1,\frac{1}{2}|\boldsymbol{M}|1,\frac{1}{2}\right\rangle=\frac{\sqrt{2}}{9}U+\frac{2}{9}T+\frac{2}{9}T', \tag{3}$$

$$\begin{aligned}\left\langle 1,-\frac{1}{2}|\boldsymbol{M}|0,\frac{1}{2}\right\rangle&=\left\langle 0,\frac{1}{2}|\boldsymbol{M}|1,-\frac{1}{2}\right\rangle\\&=\frac{1}{9}U-\frac{1}{9\sqrt{2}}T-\frac{5\sqrt{2}}{9}T',\end{aligned} \tag{4}$$

$$\left\langle 0,\frac{1}{2}|\boldsymbol{M}|0,\frac{1}{2}\right\rangle=\frac{1}{9\sqrt{2}}U-\frac{2}{9}T+\frac{7}{9}T', \tag{5}$$

where $\boldsymbol{k}_i$ and $\boldsymbol{k}_f$ in the bracket of the left-hand side are discarded to avoid confusions, since we treat only the backward scattering. Here U is the scalar amplitude and T and T' are the second-rank tensor ones which include effects of the D-component of the internal wave function of the deuteron. They are given by the invariant amplitudes as

$$U=\frac{9}{2\sqrt{2}}F\left(\frac{3}{2},\frac{3}{2},0,0\right) \tag{6}$$

and

$$T=-T_1+2T_2,\quad T'=T_1+\frac{1}{4}T_2, \tag{7}$$

where

$$\begin{aligned}T_j=&F\left(\frac{3}{2},\frac{2j-1}{2},2,0\right)-\sqrt{\frac{2}{3}}F\left(\frac{3}{2},\frac{2j-1}{2},2,1\right)\\&+F\left(\frac{3}{2},\frac{2j-1}{2},2,2\right).\end{aligned} \tag{8}$$

The numerical coefficients included in U, T, and T' are fixed so that the amplitudes have simple forms in the PWIA limit as will be seen later. The physical quantities are described by these amplitudes and for spin observables one can reduce the number of the variables by introducing the relative magnitudes and phases between them,

$$R=\frac{|T|}{|U|},\quad R'=\frac{|T'|}{|U|},\quad \Theta=\theta_T-\theta_U,\quad \Theta'=\theta_{T'}-\theta_U. \tag{9}$$

The spin observables concerned are defined in Ref. [13] as

$$T_{20}=\mathrm{Tr}(\boldsymbol{M}\tau_{20}\boldsymbol{M}^{+})/\mathrm{Tr}(\boldsymbol{M}\boldsymbol{M}^{+}), \tag{10}$$

$$\kappa_0=\frac{3}{2}\mathrm{Tr}(\boldsymbol{M}\tau_y\boldsymbol{M}^{+}\sigma_y)/\mathrm{Tr}(\boldsymbol{M}\boldsymbol{M}^{+}), \tag{11}$$

$$K_{xz}^{y}=\mathrm{Tr}(\boldsymbol{M}\tau_{xz}\boldsymbol{M}^{+}\sigma_y)/\mathrm{Tr}(\boldsymbol{M}\boldsymbol{M}^{+}), \tag{12}$$

$$K_{y}^{y}=\mathrm{Tr}(\boldsymbol{M}\sigma_y\boldsymbol{M}^{+}\sigma_y)/\mathrm{Tr}(\boldsymbol{M}\boldsymbol{M}^{+}), \tag{13}$$

$$C_{yy}=\mathrm{Tr}(\boldsymbol{M}\tau_y\sigma_y\boldsymbol{M}^{+})/\mathrm{Tr}(\boldsymbol{M}\boldsymbol{M}^{+}), \tag{14}$$

where $\boldsymbol{\tau}$ and $\boldsymbol{\sigma}$ are the spin operators for the deuteron and the proton, respectively. Inserting Eqs. (3)–(5) into the above definitions and reducing the expressions by Eq. (9), we get

$$T_{20}=\{2\sqrt{2}R\cos\Theta-R^2-32R'^2+12RR'\cos(\Theta'-\Theta)\}/N_R, \tag{15}$$

$$\kappa_0=\{\sqrt{2}-R\cos\Theta-4R'\cos\Theta'-3\sqrt{2}RR'\cos(\Theta'-\Theta)-30\sqrt{2}R'^2\}/N_R, \tag{16}$$

$$K_{xz}^{y}=3\{-R\sin\Theta+5\sqrt{2}RR'\sin(\Theta-\Theta')\}/N_R, \tag{17}$$

$$K_{y}^{y}=\frac{\sqrt{2}}{9}\{1-4\sqrt{2}R\cos\Theta+14\sqrt{2}R'\cos\Theta'+8R^2+98R'^2-56RR'\cos(\Theta-\Theta')\}/N_R, \tag{18}$$

$$C_{yy}=\frac{2\sqrt{2}}{9}\left\{1-\frac{5}{\sqrt{2}}R\cos\Theta+2\sqrt{2}R'\cos\Theta'+2R^2-70R'^2+13RR'\cos(\Theta-\Theta')\right\}\Big/N_R \tag{19}$$

with

$$N_R=\sqrt{2}+2\sqrt{2}R^2+34\sqrt{2}R'^2-4R'\cos\Theta'. \tag{20}$$

These formulas are exact and independent of details of the reaction dynamics except for the restriction by the ONE mechanism. The quantities R, R', Θ, and Θ' can be treated as free parameters such as phase shifts in usual treatments of elastic scattering [14] and will be determined by experimental data of four independent spin observables. The quantities thus obtained will be useful in finding suitable reaction models to describe the scattering.

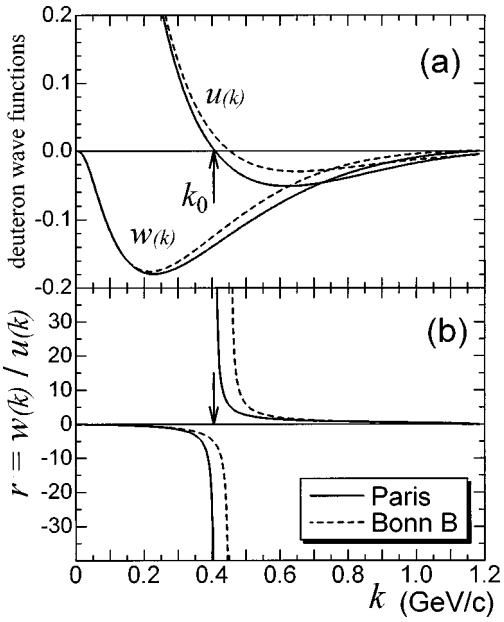

FIG. 1. Fourier transforms of deuteron internal wave functions. $u(k)$ and $w(k)$ are for the S and D components and k is the p-n relative momentum. The calculated are for the Paris (solid lines) and Bonn B (dashed lines) potentials. The zero point of $u(k)$, $k=k_0$, is shown by the arrows for the Paris potential for example.

III. ANALYSES OF THE κ_0-T_{20} CORRELATION

The experimental data available at the present are not sufficient for the determination of the four parameters R, R', Θ, and Θ' discussed in the previous section. In the following, we will calculate R and R' as the first approximation by the PWIA which is fundamentally acceptable at intermediate and high energies and treat Θ and Θ' as free parameters in the range $-180°\leqslant\Theta(\Theta')\leqslant 180°$. In this way, we will include effects of the imaginary part of the invariant amplitude in the calculation. The PWIA amplitudes for the ONE mechanism are described by $u(k)$ and $w(k)$, the Fourier transforms of the S and D components of the deuteron internal wave function. By calculating the left-hand sides of Eqs. (3)–(5) by the PWIA with the ONE assumption, we obtain

$$U=\frac{9}{\sqrt{2}}\left\{u^2(k)+\frac{1}{4}w^2(k)\right\}t(k), \tag{21}$$

$$T=\frac{9}{\sqrt{2}}u(k)w(k)t(k),\quad T'=\frac{9}{8}w^2(k)t(k), \tag{22}$$

where $t(k)$ is the proton-neutron scattering amplitude at the momentum k. Defining r by

$$r=\frac{w(k)}{u(k)}, \tag{23}$$

we get R and R' in the PWIA limit

$$R=\frac{4|r|}{4+r^2}\quad\text{and}\quad R'=\frac{r^2}{\sqrt{2}(4+r^2)}. \tag{24}$$

As is shown in Fig. 1 for typical inter-nucleon potentials, the

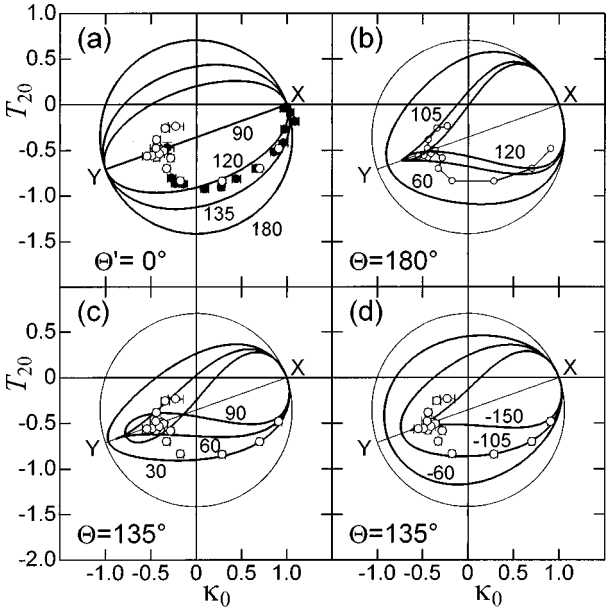

FIG. 2. T_{20} versus κ_0 ($=\frac{3}{2}K_y^y$). The experimental data are for backward elastic scattering (open circles) and inclusive breakup [solid circles, only in (a)] [7]. The curves are calculated by Eqs. (15), (16), and (20) for Θ = 180°, 135°, 120°, 90° with Θ'= 0° in (a), for Θ' = 60°, 105°, 120° with Θ=180° in (b), for Θ'=30°, 60°, 90° with Θ = 135° in (c) and for Θ'=−60°, −105°,−150° with Θ=135° in (d). The large circles are the PWIA calculation. In (b), the data points are connected by straight lines (see text).

Paris potential [16] and the Bonn B one [17], r decreases from zero to minus infinity with the increase of k, changes its sign at the zero point of $u(k)$, $k=k_0$, and beyond k_0 it decreases from plus infinity. Correspondingly, in the PWIA, $\Theta=180°$ for $k<k_0$ and $\Theta=0°$ for $k>k_0$, and Θ' is zero independently of k.

Now we will discuss the κ_0-T_{20} correlation. The calculated κ_0 and T_{20} by the use of Eqs. (15), (16), (20), and (24) are shown in Figs. 2(a)–2(d). In general case, at $r=0$,

$$T_{20}=0 \quad \text{and} \quad \kappa_0=1, \tag{25}$$

which define the point X in the κ_0-T_{20} plane in the figures. For the limit $r\to\infty$

$$T_{20}=-\frac{4\sqrt{2}}{9-\cos\Theta'} \quad \text{and} \quad \kappa_0=-\frac{7+\cos\Theta'}{9-\cos\Theta'}, \tag{26}$$

which restrict the values of T_{20} and κ_0 at $k=k_0$ independently of Θ, in the ranges

$$-\frac{1}{\sqrt{2}}\leqslant T_{20}\leqslant-\frac{2\sqrt{2}}{5} \quad \text{and} \quad -1\leqslant\kappa_0\leqslant-\frac{3}{5}. \tag{27}$$

In the pure PWIA, Eq. (26) gives $T_{20}=-1/\sqrt{2}$ and $\kappa_0=-1$ which define the point Y in the κ_0-T_{20} plane. In the figures, the spin observables are calculated for given sets of Θ and Θ', where r is varied from zero to infinity for $k<k_0$. The calculation is extended to the region $k\geqslant k_0$ by replacing $|r|$ by $-|r|$ to take account of the change of Θ at $k=k_0$.

In Fig. 2(a), the calculated T_{20} and κ_0 are plotted in the κ_0-T_{20} plane for several Θ, where Θ' is fixed to the PWIA limit, $\Theta'=0$. These quantities are independent of the sign of Θ due to Eqs. (15), (16), and (20). The point P defined by a set of κ_0 and T_{20} calculated by the PWIA moves clockwise along the circle denoted by $\Theta=180°$, from X to a certain point through Y, with the increase of k. The trajectories of the point P similarly defined for other Θ are deformed toward the inside of the circle according to the decrease of Θ from 180° to 90°, where the points for $k=k_0$ are localized in Y independently of Θ. We call this type of deformation of the trajectories the ''Θ effect.'' The experimental data [7] for the small k are mostly located between the two lines for $\Theta=120°$ and 135°. Then the Θ effect is important to describe such small k data. Figure 2(a) is essentially same as Fig. 3 in Ref. [12], because the present formulas (15) and (16) with (20) are equivalent to Eqs. (16) and (17) in the reference when $\Theta'=0$.

Figure 2(b) shows effects of the finite Θ' for typical Θ' between zero and 180°, fixing Θ to the PWIA limit, $\Theta=180°$. The calculated T_{20} and κ_0 are independent of the sign of Θ' because of $\Theta=180°$. The trajectories of P for the finite Θ' are deformed to form an egg shape ($\Theta'=60°$), a cusp-like shape ($\Theta'=105°$) (hereafter we will call this type the ''cusp'') or an ''eight'' shape ($\Theta'=120°$) although the last one is laid down and one loop is very small. The point P for $k=k_0$, which is defined by Eq. (26), moves on the X-Y straight line from Y toward the point ($T_{20}=-2\sqrt{2}/5$, $\kappa_0=-3/5$), with the increase of the magnitude of Θ'. We will call such effects the ''Θ' effect.'' Most of the data for large k are localized between the lines for $\Theta'=105°$ and 120° and the Θ' effect is clearly important to reproduce such high-energy data. As will be seen later, the cusp and the eight shape are successful to describe the experimentally observed structure of T_{20} in the plot against k.

Figures 2(c) and 2(d) show the combination of the Θ effect and the Θ' one, for $\Theta'>0$ and $\Theta'<0$, respectively, with fixing Θ to 135°. In Fig. 2(c), the trajectories for $\Theta'>90°$ are ignored to avoid the complication of the figure. The combination of the Θ effect and the Θ' one improves the T_{20}-κ_0 correlation. For example in the cases of $\Theta'=30°$ and $-105°$, the agreement between the calculation and the experiment is much better than that in the PWIA.

In the analyses, the trajectories of the point P are symmetric about the X-Y straight line, which is proved by Eqs. (15), (16), (20), and (24), and it should be emphasized that the above results are independent of a particular choice of the nuclear potential. The validity of the PWIA estimation of R and R' is examined by varying them as $R\to R+\Delta R$ and $R'\to R'+\Delta R'$. When ΔR and/or $\Delta R'$ are $\pm10\%$ of their originals, no real effect is produced by the variation in the correlation curves. The effects are examined up to the 50% variation, for which the effects are appreciable but still small. In Figs. 3(a)–3(d), the results for the case of 30% variation are shown as examples for the typical trajectories by $(\Theta,\Theta')=(135°,30°)$, $(135°,-105°)$, $(180°,105°)$, $(180°,120°)$. Therefore, the use of Eq. (24) will not induce significant errors.

IV. MOMENTUM DEPENDENCE OF THE SPIN OBSERVABLES

To examine the Θ and Θ' effects in more detail, we will investigate the dependence of the spin observables on the

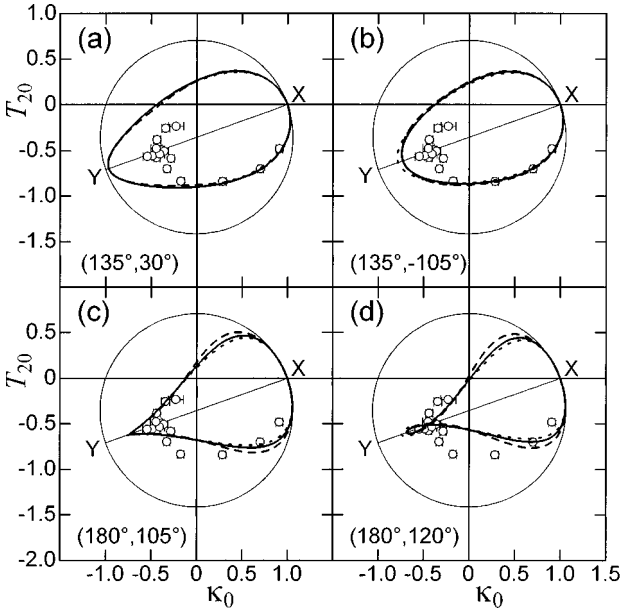

FIG. 3. Effects of variations of R and R' on the κ_0-T_{20} correlation. The effect of the variation of R (R'), $R \rightarrow R+\Delta R$ ($R' \rightarrow R'+\Delta R'$), is shown by the dashed (dotted) lines with $\Delta R/R$, $\Delta R'/R' = 0.3$ for the typical sets of (Θ, Θ'), (135°, 30°) (a), (135°, −105°) (b), (180°, 105°) (c) and (180°, 120°) (d). The solid lines are for $\Delta R = \Delta R' = 0$. The experimental data are taken from Ref. [7].

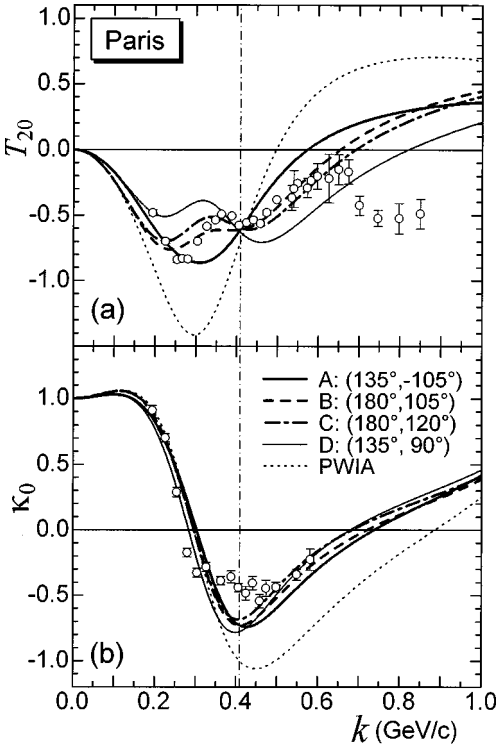

FIG. 4. T_{20} (a) and κ_0 (b) versus k. The curves are calculated by Eqs. (15), (16), and (20) with the Paris potential, where the lines are for $(\Theta, \Theta') = (135°, -105°)$ [set A, the solid], (180°, 105°) [set B, the dashed], (180°, 120°) [set C, the dash-dotted] and (135°, 90°) [set D, the thin solid]. The thin dotted lines are for the PWIA calculation. The vertical dash-dotted straight line indicates the location of $k = k_0$. The experimental data are taken from Refs. [7,18].

proton-neutron relative momentum k. We calculate r by the use of Eq. (23), where $u(k)$ and $w(k)$ are obtained by assuming a particular potential. Recently, relativistic effects on the wave function of the deuteron internal motion have been investigated by the use of the Bethe-Salpeter equation [15] and the effects are found to be small in the present p-n relative momentum range when compared to the nonrelativistic wave functions by the Paris potential [16]. Then, in most of our cases, the results are given for the Paris potential and those for other potentials will be described briefly.

Shown in Figs. 4(a) and 4(b) are T_{20} and κ_0 by the Paris potential as the functions of k for the typical trajectories in Figs. 2(b)–2(d), i.e., for the sets $(\Theta, \Theta') = (135°, -105°)$(A), (180°, 105°)(B), (180°, 120°)(C), (135°, 90°)(D) and for the pure PWIA. The trajectory for set A is the egg shape and the one for B is the cusp and those for C and D are the eight shape, respectively. As seen in Fig. 4(a), the calculation by set A reproduces well the low k data of T_{20} but does not produce the resonancelike structure of T_{20}, which is observed experimentally as a local maximum in the range $k = 0.25 \sim 0.45$ GeV/c [7]. On the other hand, the calculations for other three sets describe the feature of the observed structure. Thus the cusp or eight shape trajectory in the κ_0-T_{20} plane will be required to reproduce the structure in the plot of T_{20} against k. This is confirmed by the detailed examination of the behavior of the experimental data in the plane, i.e., the data behave as a cusp upon the X-Y line as emphasized by connecting the data points with the straight lines in Fig. 2(b). The calculations by sets B and C are successful in reproducing the gross behavior of the experimental data [7], except the data at $k \geqslant 0.7$ GeV/c [18]. In the figure, the calculated T_{20} at $k = k_0$ are localized independently of Θ in a narrow range around $T_{20} = -0.6$ almost as one point. This will be explained by the theoretical restriction on T_{20} given by Eq. (26) and the good agreement between the calculations and the experimental data at this momentum will support the present theory. As in Fig. 4(b), the calculated κ_0 agrees with the experimental data [7] better than the PWIA, particularly for the large k.

Similar calculations of T_{20} and κ_0 are performed for the traditional nuclear potentials, the RSC [19], Nijmegen [20], AV14 [21], and Bonn B [17] ones and for the recently proposed Nijmegen II potential [22]. The observables calculated by the Nijmegen II potential are quite similar to those by the Paris potential and both results are hardly distinguished to each other. Other potentials except for the Bonn B provide almost similar results, but with some variations in the AV14 case in a high momentum region, compared to those by the Paris and Nijmegen II potentials. However, as is seen in Fig. 1(b), the k dependence of r for the Bonn B potential is considerably shifted toward larger k compared with that for the Paris potential. This nature will be understood through the behavior of $u(k)$ and $w(k)$ in Fig. 1(a) by the characteristics of the Bonn B potential which has rather weak tensor parts and complementarily strong central ones. Considering this speciality, the results for the Bonn B case are compared with the experimental data in Figs. 5(a) and 5(b). The quality of the agreement between the calculation and the experiment is almost similar to that in the case of the Paris potential. As is shown in Eq. (27), the magnitude of the calculated κ_0 at $k = k_0$ is limited in the range, $-1 \leqslant \kappa_0 \leqslant -0.6$, which is inde-

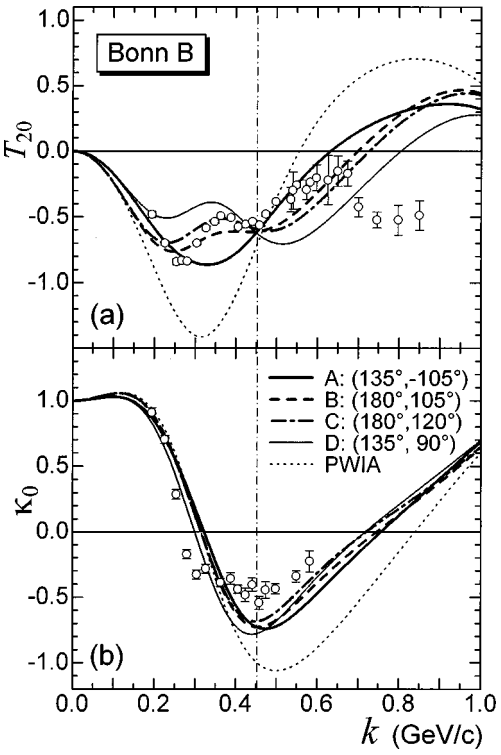

FIG. 5. The same as Fig. 4 except for the use of the Bonn B potential.

pendent of the choice of Θ. In this viewpoint the present experimental data seem to favor the Bonn B potential since the lower bound of the measured κ_0 is almost -0.6, which will be given by the Bonn B potential as the upper limit at $k=k_0$ when $\Theta'=180°$. However, it will not be suitable at the present to discuss in detail the superiority between the nuclear potentials, because of the ambiguity of the experimental data and the approximation in the calculation.

Next we will investigate in general way the Θ effect and the Θ' one on the momentum-dependence of T_{20} and κ_0. First we will examine the Θ' effect by calculating the following combination of T_{20} and κ_0, which is independent of Θ:

$$T_{20}+2\sqrt{2}\kappa_0=\frac{4}{N_R}\left\{1-\frac{1}{4}R^2-38R'^2-2\sqrt{2}R'\cos\Theta'\right\}. \tag{28}$$

Figure 6 describes this quantity as the function of k for several Θ' for the Paris potential. Here, the experimental data around $k=k_0$ are reproduced well by large Θ', for example $\Theta'=180°$. Then, in the following examination of the Θ effect, we fix Θ' to 180°. The calculated T_{20} and κ_0 for several Θ are shown for the Paris potential in Figs. 7(a) and 7(b) as the function of k. The small Θ, for example $\Theta=0°$ with $\Theta'=180°$, which we will call set E, describes well the T_{20} data at large k but unfortunately does not those at small k. In the figure, the calculated T_{20} and κ_0 are independent of Θ at about $k=0.3$ GeV/c, 0.6 GeV/c, which correspond to $r=\pm\sqrt{2}$, and at $k=k_0$. There the magnitude of the calculated T_{20} at $k\simeq 0.3$ GeV/c is only about one half of the measured. Then the choice of $\Theta'=180°$ is not suitable to describe such low k data contrary to the success at $k\geqslant k_0$, independently of

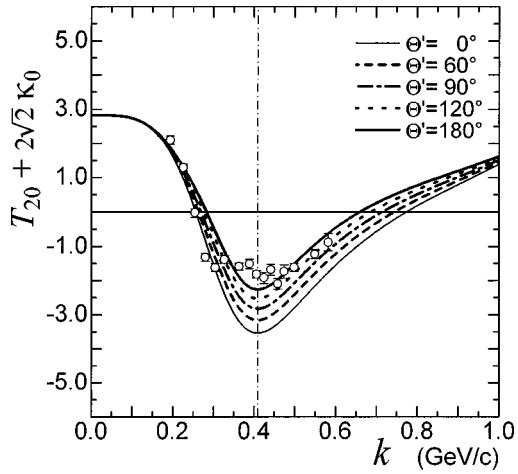

FIG. 6. $T_{20}+2\sqrt{2}\kappa_0$ versus k. The calculation with the Paris potential is shown for $\Theta'=0°$ (thin solid line), 60° (dashed line), 90° (dash-dotted line), 120° (dotted line), and 180° (solid line). The PWIA calculation is the same as that for $\Theta'=0°$. It should be noted that the calculated quantity is independent of Θ (see text). The vertical dash-dotted straight line indicates the location of $k=k_0$. The experimental data are taken from Refs. [7,18].

the choice of Θ. This indicates that one cannot reproduce all of the data of T_{20} and κ_0 with one set of Θ and Θ'.

In the present paper, we consider the contribution of open channels other than the elastic scattering as the absorption effect, which is taken into account by the imaginary parts of the invariant amplitudes through the relative phases between

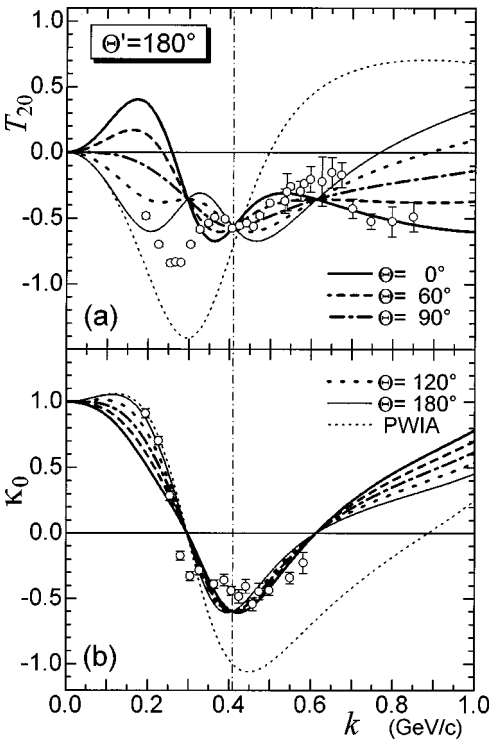

FIG. 7. Θ dependence of T_{20} (a) and κ_0 (b). The solid, dashed, dash-dotted, dotted, and thin solid lines are for $\Theta=0°$, 60°, 90°, 120°, and 180°, respectively. The thin dotted lines are for the PWIA. The Paris potential is used and $\Theta'=180°$. The vertical dash-dotted straight line indicates the location of $k=k_0$. The experimental data are taken from Refs. [7,18].

the amplitudes, Θ and Θ'. On the other hand, the magnitudes of the amplitudes are fixed to those calculated by the PWIA. However, the elimination of the open channels will affect the magnitudes as well as the phases. Also, the deuteron-proton rescattering before and/or after the ONE process will contribute to the magnitude although expected to be small at high energies. These effects will give the correction to the PWIA estimation of R and R'. The PWIA estimation is decomposed into the two steps, i.e., the calculation of R and R' as the functions of the parameter r by Eq. (24) and the calculation of r as the function of k through the deuteron internal wave functions by the use of $r=w(k)/u(k)$. The validity of the first step has been examined in the previous section. Since r is a measure of the magnitudes of the scattering amplitudes, we will investigate effects due to variations of r, which will be described by an additional correction term to $w(k)/u(k)$. In general, such corrections will vary with the incident energy, namely, of the momentum k, for example the open-channel effects increase with k. Having these in mind, we will assume the general form of variations of r as

$$r \rightarrow r+\Delta r, \quad \Delta r = a(k/k_{\max})^n. \tag{29}$$

We will call Δr simply the ''momentum-dependent correction,'' although this allows the momentum-independent case by the choice $n=0$. The quantities T_{20} and κ_0 calculated by the use of Eq. (29) with r obtained by the Paris potential are shown, for example for set C, in Figs. 8(b) and 8(c). The parameters are chosen, for simplicity, as $n=1$, $k_{\max}=1.0$ GeV/c and $a=\pm 1.5$. As is shown in Fig. 8(a), the modification induced on r is rather small for these parameters. However, the correction due to the variation of r brings about large effects on T_{20} and κ_0 except for the momentum region around $k=k_0$. In particular, the calculated T_{20} becomes negative at $k \geqslant 0.7$ GeV/c due to this effect. The calculation without this correction gives positive T_{20} at $k \simeq 0.7-1.0$ GeV/c and does not reproduce the T_{20} data which is negative in this momentum region. Then, the effect of the momentum-dependent correction will be one candidate to solve such discrepancies between the calculation and the measurement, when a proper k dependence is assumed for Δr. Similar results are obtained by the use of the Bonn B potential. It should be emphasized that the modification of r does not induce any change in the trajectories described in Figs. 2(a)–2(d), because the trajectories are calculated by treating r as the free parameter and are independent of the determination of r as the function of k.

Other spin observables, K_{xz}^y, K_y^y, and C_{yy} are investigated by the use of the Paris potential in two ways; i.e., the dependence of these quantities on Θ and Θ' are shown in Figs. 9(a)–9(c), for the sets of Θ and Θ', A, C, D, and E and the effects of the momentum-dependent correction are shown in Figs. 10(a)–10(c) for set C with $n=1$, $k_{\max}=1.0$ GeV/c and $a=\pm 1.5$. The results by set B are not displayed because of similar nature of the results to those by set C. Figure 9(a) shows that the calculated K_{xz}^y is quite sensitive to the choice of Θ and Θ' and, in particular, the sign of K_{xz}^y in a region of k around k_0 depends on the sign of Θ'. Also, K_{xz}^y vanishes for set E and for the PWIA calculation. Thus measurements of this quantity will give a clear test of the (Θ, Θ') sets.

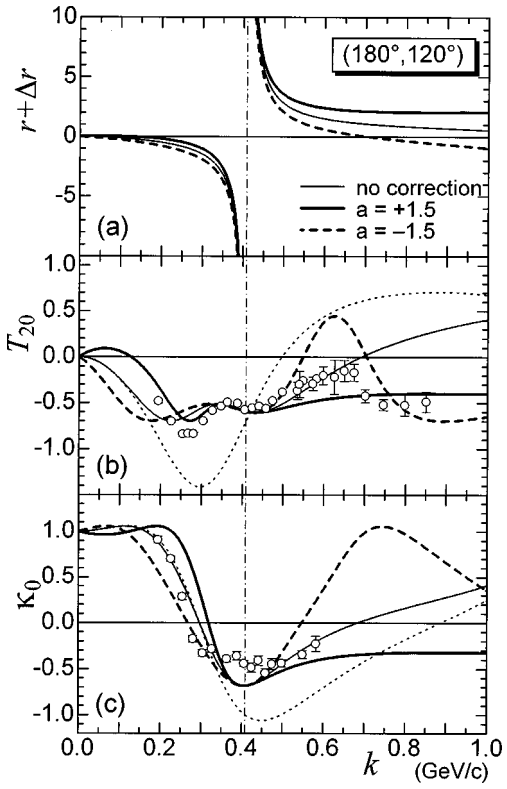

FIG. 8. Effects of variations of r on T_{20} and κ_0. The variation of r, the effects on T_{20} and those on κ_0 are shown in (a), (b), and (c), respectively, where the case of $n=1$, $k_{\max}=1.0$ GeV/c and $a=1.5$ (-1.5) is described by the solid (dashed) lines. The thin solid lines are for $a=0$ and the thin dotted lines are for the PWIA calculation. The vertical dash-dotted straight lines indicates the location of $k=k_0$. The experimental data are taken from Refs. [7,18].

Also, K_{xz}^y vanishes at $k=k_0$ due to $R=0$, independently of the choice of Θ and Θ'. This will be useful in criticizing the nuclear potential, because the magnitude of k_0 depends on the potential assumption. The quantities K_y^y and C_{yy} are less sensitive to Θ and Θ' compared with K_{xz}^y but will be still useful to identify the Θ and Θ' effects. As is seen in Fig. 10(a)–10(c), the effect of the variation of r appears in all of these quantities, remarkably in K_{xz}^y. Then the measurement of K_{xz}^y will be useful to distinguish the superiority in explaining the data between the sets of Θ and Θ' as well as between the nuclear potentials and to identify the effect of the momentum-dependent correction at the high energies.

V. SUMMARY AND DISCUSSIONS

For the dp backward elastic scattering, the present paper provides the formulas of T_{20}, κ_0, K_{xz}^y, K_y^y, and C_{yy}, which are free from details of the reaction dynamics except for the ONE assumption. There nonexchange scattering is neglected as the conventional treatments [1–6] because of small contributions at the backward angle due to high energies. The correlation between T_{20} and κ_0 is analyzed by introducing the imaginary parts of the invariant amplitudes which are parametrized by the relative phases between the scalar amplitude and the tensor ones, Θ and Θ', and reasonable understanding of the experimental data is given by choosing suitable sets of Θ and Θ'. The momentum (k) dependence

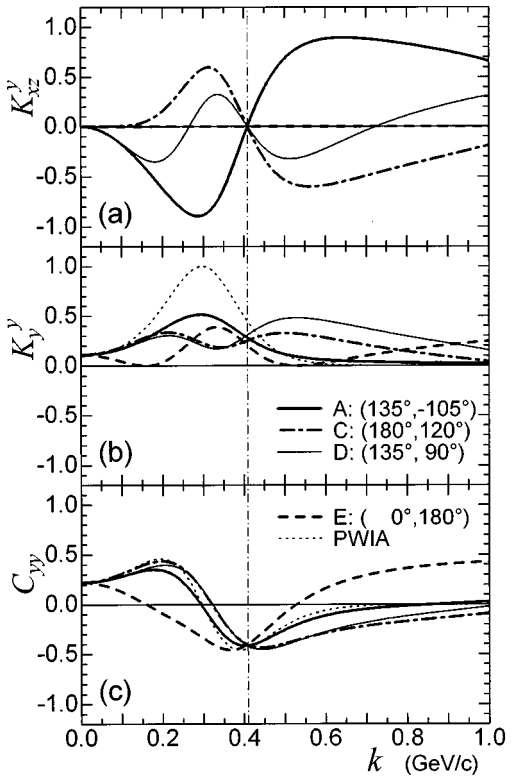

FIG. 9. K^y_{xz}, K^y_y, and C_{yy} versus k. The calculation of K^y_{xz} (a), K^y_y (b), and C_{yy} (c) with the Paris potential are shown for the (Θ,Θ') sets, A, C, D, and E by the solid, dash-dotted, thin solid, and dashed lines, respectively. The thin dotted lines are for the PWIA calculation. The vertical dash-dotted straight line indicates the location of $k=k_0$.

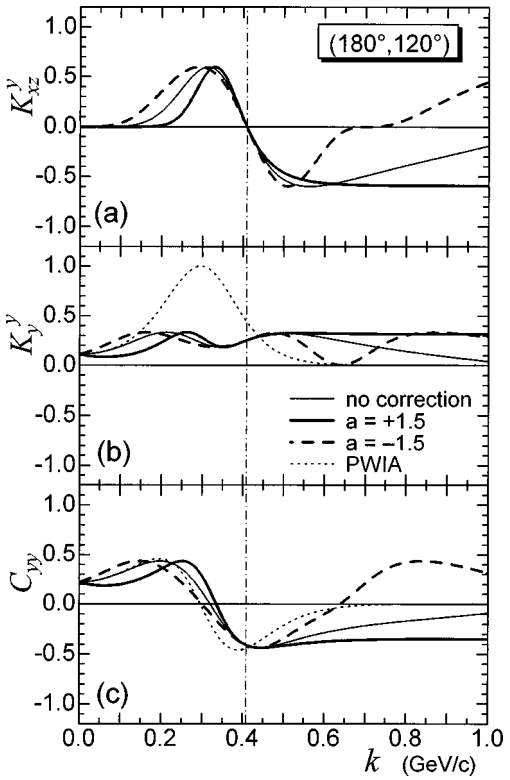

FIG. 10. Effects of variations of r on spin observables. The calculation of K^y_{xz} (a), K^y_y (b), and C_{yy} (c) with the Paris potential are shown for set C with $n=1$, $k_{max}=1.0$ GeV/c and $a=1.5$ (-1.5) by the solid (dashed) lines. The thin solid lines are for $a=0$ and thin dotted lines are for the PWIA calculation. The vertical dash-dotted straight line indicates the location of $k=k_0$.

of the spin observables is calculated by assuming several nuclear potentials and most of the experimental data are reproduced by the sets of Θ and Θ' which explain the correlation data. In particular, Θ and Θ' which produce the cusp or eight shape trajectories in the κ_0-T_{20} plane are successful in describing the structure of T_{20} in the plot against k in the medium momentum region. Such successful results will support the assumption of the ONE mechanism which includes the absorption effects. By treating Θ and Θ' as free parameters and including the corrections to the PWIA estimates of R and R', the present calculation takes into account, in principle, contributions of many Feynman graphs, which contain the simple ONE diagram and ONE diagrams accompanied by networks of deuteron breakup, emission and absorption of mesons including excitations of nucleons, deuteron-proton rescattering, and so on. In these corrections, still we assume the validity of vanishing of the matrix element $\langle 1,-\frac{1}{2}|\boldsymbol{M}|1,-\frac{1}{2}\rangle$, which is justified in the case of the mesonic effects considered in Ref. [3].

In the present investigation, we assume Θ and Θ' to be independent of k for the convenience of examining the general effect of the imaginary part of the amplitudes. In general, Θ and Θ' will vary with the incident energy, namely, with k. Then, to reproduce the experimental data quantitatively, one will vary Θ and Θ' with k, for example by adopting set A $(\Theta=135°,\Theta'=-105°)$ for the low k region and set B or C $(\Theta=180°,\Theta'=105°\sim120°)$ for the medium k region. The important factor of set A is the Θ effect, as is discussed for Fig. 2 (a), and physically the effect will be induced by non-mesonic reactions like virtual breakup of the deuteron [23], because the low k region is below the pion threshold. Considering U, T, and T' in the PWIA limit, the virtual breakup process contributes mainly to U and T and the contribution to T' will be very small because the magnitude of $w(k)$ is small compared to that of $u(k)$ in this momentum region. Then the main effect of the virtual breakup will be described by the Θ effect. Earlier the structure of T_{20} in the plot against k in the medium momentum region has been interpreted as mesonic effects which include virtual excitations of the nucleons to baryon resonance states [1–3]. The large magnitude of Θ' in set B or C will be understood as the reflection of such mesonic phenomena. The virtual emission of mesons contributes to U and T', but hardly to T, because the emission does not induce the interference between the S and D components of the deuteron wave function, when the recoil of the related nucleons is neglected. The sets of Θ and Θ', A, B and C, do not reproduce the T_{20} data at $k\geqslant0.7$ GeV/c, while the set E $(\Theta=0°,\ \Theta'=180°)$ reproduces the data very well. When set E is adopted in this momentum region, for explaining the drastic changes of Θ and Θ' from set B or C around $k=k_0$, it will be necessary to assume the participation of new phenomena, for example, excitations of higher baryon resonance states accompanied by related dynamical effects.

The validity of the PWIA estimation of R and R' is investigated. Decreases or increases of R and R' by up to 50 %

do not produce any significant effect on the κ_0-T_{20} correlation. However, the small variation of r due to the momentum-dependent correction gives large effects on most of the spin observables. The calculation suggests that the theoretical T_{20} at the high energies is possibly improved by taking account of this correction. On the other hand, the calculated T_{20} at the high energies is very sensitive to the position of the zero point of $w(k)$ on the k-axis. For example, $w(k)$ calculated by the simple Bonn potential has the zero point at about $k=0.8$ GeV/c [15] and the PWIA calculation with this potential gives negative T_{20} for $k \geqslant 0.8$ GeV/c [18]. Thus, a suitable potential which produces the zero point at $k \simeq 0.7$ GeV/c will give a solution for the high-energy T_{20} problem. When referred to the relation between $w(k)$ and r in Fig. 1, it is speculated from the behavior of r in Fig. 8(a) that the spin observables in this case will qualitatively resemble those by the momentum-dependent correction with $a=-1.5$, which are given in Figs. 8 and 10. Due to such variety of the possible solutions at the high energies, we need more information from experiments to get the definite conclusion and, in this sense, it is desirable to measure other spin observables, for example κ_0 and K_{xz}^{y}, at the energies concerned.

ACKNOWLEDGMENTS

The authors wish to thank Professors Y. Koike and T. Hasegawa for valuable discussions and are indebted to Professor C. F. Perdrisat for providing the details of his data.

[1] J. Arvieux *et al.*, Nucl. Phys. **A431**, 613 (1984), and references therein.
[2] A. Boudard and M. Dillig, Phys. Rev. C **31**, 302 (1985).
[3] A. Nakamura and L. Satta, Nucl. Phys. **A445**, 706 (1985).
[4] A. P. Kobushkin, J. Phys. G **12**, 487 (1986).
[5] S. S. Vasan, Phys. Rev. D **8**, 4092 (1973).
[6] A. P. Kobushkin *et al.*, Phys. Rev. C **50**, 2627 (1994).
[7] V. Punjabi *et al.*, Phys. Lett. B **350**, 178 (1995).
[8] B. D. Keister, Phys. Rev. C **24**, 2628 (1981); B. D. Keister and J. A. Tjon, *ibid.* **26**, 578 (1982).
[9] I. M. Sitnik, V. P. Ladygin, and M. P. Rekalo, Phys. At. Nucl. **57**, 2089 (1994); Yu. L. Dorodnykh and V. M. Kolybasov, Phys. Lett. B **333**, 283 (1994); B. Kuehn, C. F. Perdrisat, and E. A. Strokovsky, Phys. At. Nucl. **58**, 1795 (1995); L. P. Kaptari *et al.*, Phys. Lett. B **351**, 400 (1995); A. P. Kobushkin and A I. Syamtomov, Few-Body Syst., **8**, 364 (1995).
[10] P. P. Rekalo and I. M. Sitnik, Phys. Lett. B **356**, 434 (1995).
[11] M. Tanifuji and K. Yazaki, Prog. Theor. Phys. **40**, 1023 (1968).
[12] M. Tanifuji, Phys. Lett. B **363**, 151 (1995).
[13] G. G. Ohlsen, Rep. Prog. Phys. **35**, 717 (1972).
[14] M. Tanifuji, Phys. Lett. B **289**, 233 (1992); M. Tanifuji and H. Kameyama, Nucl. Phys. **A602**, 1 (1996).
[15] L. P. Kaptari *et al.*, Phys. Rev. C **54**, 986 (1996).
[16] M. Lacombe *et al.*, Phys. Rev. C **21**, 861 (1980).
[17] R. Machleidt, Adv. Nucl. Phys. **19**, 189 (1989).
[18] L. S. Azhgirey *et al.*, Phys. Lett. B **391**, 22 (1997).
[19] R. V. Reid, Ann. Phys. (N.Y.) **50**, 411 (1968).
[20] M. M. Nagels, T. A. Rijken, and J. J. de Swart, Phys. Rev. D **17**, 768 (1978).
[21] R. B. Wiringa, R. A. Smith, and T. L Ainsworth, Phys. Rev. C **29**, 1207 (1984).
[22] V. G. J. Stoks, R. A. M. Klomp, C. P. F. Terheggen, and J. J. de Swart, Phys. Rev. C **49**, 2950 (1994).
[23] M. Yahiro, Y. Iseri, H. Kameyama, M. Kamimura, and M. Kawai, Prog. Theor. Phys. Suppl. **89**, 32 (1986); Y. Iseri, M. Tanifuji, H. Kameyama, M. Kamimura, and M. Yahiro, Nucl. Phys. **A533**, 574 (1991).